Fluorescence Spectroscopy

DOI: 10.1002/ange.200800528

Defect-Mediated Photoluminescence Dynamics of Eu^{3+}-Doped TiO_2 Nanocrystals Revealed at the Single-Particle or Single-Aggregate Level**

*Takashi Tachikawa, Takamasa Ishigaki, Ji-Guang Li, Mamoru Fujitsuka, and Tetsuro Majima**

Lanthanide-doped materials are finding use in a wide variety of applications in optics as gain media for amplifiers and lasers and as biolabels, white-light emitters, and full-color phosphors for displays.[1,2] Since direct excitation of the parity-forbidden intra-f-shell lanthanide ion crystal-field transitions is inefficient, it is anticipated that the luminescence of lanthanide ions incorporated in a wide-band-gap semiconductor lattice (e.g., ZnO and TiO_2) could be sensitized efficiently by exciton recombination in the host (Figure 1). Recently, we synthesized Eu^{3+}-doped TiO_2 (TiO_2:Eu^{3+}) nanocrystals by Ar/O_2 radio-frequency thermal plasma oxidation and observed bright red emission either by exciting the TiO_2 host with UV light of shorter wavelength than 405 nm or by directly exciting Eu^{3+} at a wavelength beyond the absorption edge (405 nm, 3.06 eV) of TiO_2. Various types of defect states have been considered to play an important role in energy transfer between TiO_2 and the activating Eu^{3+} ions. For example, with increasing annealing temperature, the photoluminescence (PL) intensity of visible emissions due to Eu^{3+} ions increases at first but then decreases and reaches a maximum at an annealing temperature of 700 °C.[2c] In this respect, the luminescence of Eu^{3+} depends critically on the locations of dopants in the host. However, the mechanism of the energy-transfer process from the defect energy levels of the host to dopants has not yet been clarified owing to several difficulties, such as the inhomogeneous distribution of ions in the material.

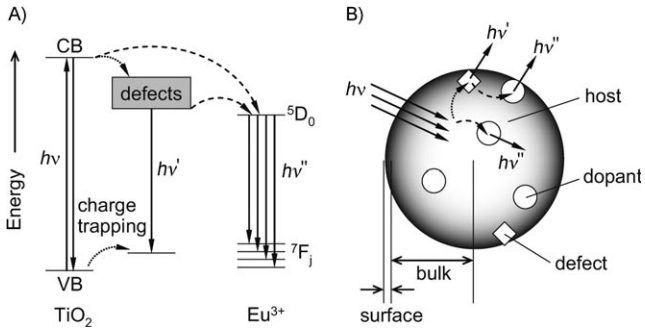

Figure 1. A) Energy diagram for the charge- and energy-transfer reactions induced by photoexcitation of TiO_2:Eu^{3+} nanoparticles. VB and CB denote valence and conduction bands, respectively. The charge-trapping and energy-transfer processes are indicated by the dotted and dashed arrows, respectively. B) Illustration of energy transfer from the TiO_2 host to the doped Eu^{3+} ions. The Eu^{3+} ions located in the interior region and at the surface of the TiO_2 host are sensitized efficiently by exciton recombination.

[*] Dr. T. Tachikawa, Prof. Dr. M. Fujitsuka, Prof. Dr. T. Majima
The Institute of Scientific and Industrial Research (SANKEN)
Osaka University, Mihogaoka 8-1, Ibaraki, Osaka 567-0047 (Japan)
Fax: (+81) 6-6879–8499
E-mail: majima@sanken.osaka-u.ac.jp
Homepage:
http://www.sanken.osaka-u.ac.jp/labs/mec/index.html
Prof. Dr. T. Ishigaki, Dr. J.-G. Li
National Institute for Materials Science, Nano Ceramics Center
Namiki 1-1, Tsukuba, Ibaraki 305-0044 (Japan)

[**] This work has been partly supported by a Grant-in-Aid for Scientific Research (Project 17105005 and others) from the Ministry of Education, Culture, Sports, Science and Technology (MEXT) of Japanese Government. T.T. is thankful for partial support from the Iketani Science and Technology Foundation.

Supporting information for this article is available on the WWW under http://dx.doi.org/10.1002/anie.200800528.

Single-molecule (single-particle) fluorescence spectroscopy has already yielded new insight into the photophysics and photochemistry of inorganic and organic nanocrystals.[3] There are, however, only a few reports on the PL behavior of lanthanide-doped materials.[4] We have now investigated the PL dynamics of undoped TiO_2 and TiO_2:Eu^{3+} (0.5 atom %) nanoparticles (or their aggregates) using single-particle PL spectroscopy. Photostimulated formation of emissive defects at the TiO_2 surface and defect-mediated PL of the doped Eu^{3+} were examined at the single-particle or single-aggregate level.

Undoped TiO_2 and TiO_2:Eu^{3+} powders were synthesized by radio-frequency Ar/O_2 thermal-plasma oxidation of mists of liquid precursors containing titanium tetra-*n*-butoxide and europium nitrate. Detailed synthetic procedures and characterization of particles (UV/Vis absorption and excitation spectra, XRD, TEM, and AFM) are given in reference [2d] and the Supporting Information.

The PL images and spectra of individual luminescent spots were measured during 405-nm laser excitation of TiO_2:Eu^{3+} nanoparticles in ambient air. As shown in Figure 2A, a number of spots with various intensities were observed (left image).

Figure 2B shows typical PL spectra of individual luminescent spots below the diffraction limit of about 150 nm for TiO_2:Eu^{3+} nanoparticles in ambient air (the AFM image is given in the Supporting Information, Figure S1). Single-particle spectral measurements revealed that the PL bands around 590 and 615 nm are attributable to transitions from the $^5D_0$ level to the $^7F_1$ and $^7F_2$ levels of Eu^{3+}, respectively.[1,2] Since the $^5D_0 \rightarrow {}^7F_2$ transition is electrically allowed, it is very sensitive to the surroundings of the Eu^{3+} ion, whereas the

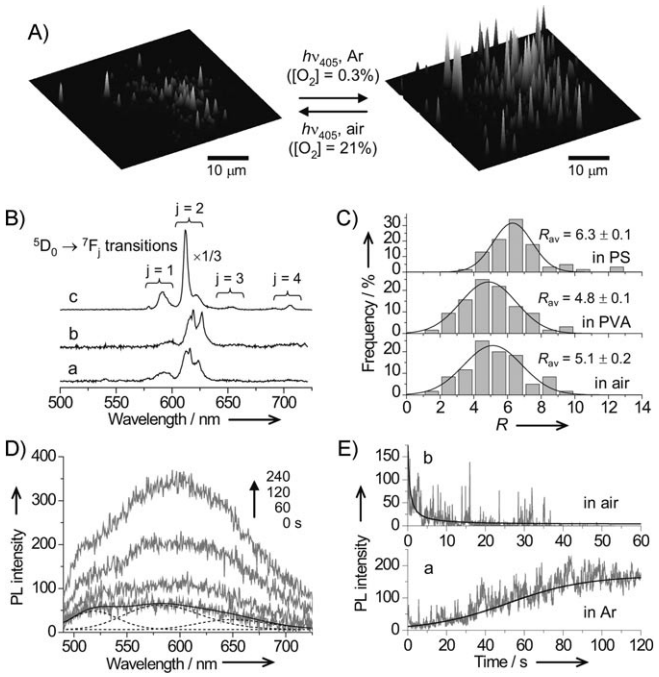

Figure 2. A) Typical PL images observed during 405-nm laser excitation for TiO_2:Eu^{3+} nanoparticles (or aggregates) under air (left) and Ar (right) atmospheres. B) Typical PL spectra of individual TiO_2:Eu^{3+} nanoparticles (or aggregates) in ambient air. C) Histograms of the *R* values obtained for single TiO_2:Eu^{3+} nanoparticles (or aggregates) spin-coated on the cover glass (dry sample; RH ≈ 40%) (a), embedded in a PVA film (b), and surface-modified nanoparticles embedded in a PS film (c). Average *R* values were determined from the Gaussian fits. D) Time evolutions of the PL spectra obtained during 405-nm laser excitation for a single undoped TiO_2 nanoparticle (or aggregate) under an Ar atmosphere. The dotted lines indicate the Gaussian distributions fitted to the spectrum (see text for details). E) Trajectories of PL intensities under Ar (a) and air (b) atmospheres (bin time is 33 ms). Solid lines indicate the kinetic traces calculated by using Equation (1).

magnetically allowed $^5D_0 \rightarrow {}^7F_1$ transition is almost not influenced. Consequently, the relative intensity (area) ratio of $^5D_0 \rightarrow {}^7F_2$ to $^5D_0 \rightarrow {}^7F_1$, the so-called *R* value, provides information about the breaking of centrosymmetry and the degree of disorder around the Eu^{3+} ions.[1,2] For instance, a relatively small *R* value (2.8) was obtained for spectrum a compared with that of 7.8 for spectrum b. In addition, 5% of the particles showed blue-shifted emission (spectrum c), which may be assignable to $Eu_2Ti_2O_7$ particles,[2d] because the fraction of such particles increased with increasing concentration (5 atom%) of doped Eu^{3+} (data not shown). Thus, we excluded all $Eu_2Ti_2O_7$ particles from the following statistical analyses.

As shown in Figure 2C, a very wide *R* distribution was obtained. This result clearly indicates that the local environment around the doped Eu^{3+} ions in TiO_2 is quite different between individual nanoparticles. According to the average particle size (ca. 10 nm, Figure S1), the number of Eu^{3+} ions per single particle and interion distance are roughly estimated to be 230 and 0.8 nm on average, respectively.[5] As suggested elsewhere, the luminescence properties are significantly influenced by dopant-pair formation.[1,6] For example, the emission from higher ^5D_j levels of Eu^{3+} or Tb^{3+} is quenched by cross-relaxation processes in pairs, whereas this is not observed for single ions.[1] Based on the mathematical probabilistic theory (Stein–Chen Poisson approximation),[7] the probability for pair-state formation is calculated to be 26% (see Supporting Information for details). These estimates imply that several emitting sites exist in the interior region and at the surface of the nanoparticles.[8]

The TiO_2 nanoparticles are usually covered with hydroxyl groups and physisorbed water molecules. Dossot and coworkers recently reported that the *R* value of about 4 obtained for the Eu^{3+}-doped glass sample can be assigned to partially hydroxylated Eu^{3+} ions with Eu–OH bonds.[9] In fact, almost the same distribution of *R* values was obtained for the TiO_2:Eu^{3+} nanoparticles in a poly(vinyl alcohol) (PVA) film, that is, the TiO_2 surface is covered with hydroxyl groups in ambient air (Figure 2C). When the TiO_2 surface was modified with octadecyltrimethoxysilane,[10] the distribution of *R* values shifted to higher values and became narrower relative to the PVA-coated sample. From these findings, it is considered that the Eu^{3+} ions located at the surface have a lower *R* value than those in the interior region of the TiO_2 host in ambient air.[11]

Interestingly, as shown in Figure 2A, a dramatic increase in PL intensity was observed on changing the gas atmosphere from air to Ar during laser irradiation for TiO_2:Eu^{3+} nanoparticles (and vice versa). A reversible change in PL intensity was also observed for undoped TiO_2 nanoparticles. The spectral measurements clearly show growth of a broad PL band in the visible region (500–750 nm), which can be assigned to the oxygen-vacancy-related defects (color centers; see Figure 2D).[12,13]

Photoactivation of nanoparticle PL, that is, an increase in intensity by an order of magnitude or more, is a new process of preparing highly luminescent nanocolloids, such as semiconductor quantum dots.[14] In our system, light absorption in the spectral region of the intrinsic absorption ($h\nu >$ 3.06 eV)[2d] and in the bands corresponding to the color centers (extrinsic absorption, $h\nu < 3.06$ eV) generates free electrons that induce formation of free and trapped excitons and surface oxygen species, such as the superoxide radical anion ($O_2^{\bullet -}$), which oxidize the color centers.[13,15]

According to the literature,[13] the main feature of the kinetics under visible-light irradiation is the dependence of the absorbance of the sample on the number of color centers (*N*). Assuming that the rates of formation (k^+) and deactivation (k^-) of the color centers are directly proportional to *N*, one obtains Equation (1), where N_0 is the number of color centers that exist prior to irradiation.[13]

$$N(t) = \frac{1}{\frac{k^+}{k^-} - \left(\frac{k^+}{k^-} - \frac{1}{N_0}\right)\exp(-k^+ t)} \qquad (1)$$

The observed trajectories of the PL intensity were well reproduced by Equation (1) (see Figures 2E and S2). Although it is very difficult to estimate the absolute value, the N_0 values significantly increased by a factor of about 20 after the photoactivation.[16,17] Assuming that the absorption cross section and PL quantum yield of color centers are

constant, the k^+ value is determined to be $0.05 \pm 0.01\ s^{-1}$ for both processes, while the k^- values are 0.5 ± 0.2 and $15 \pm 5\ s^{-1}$ for the photoactivation and deactivation processes, respectively. The remarkable difference in k^- should be due to the different oxygen concentration in the gas phase.

In addition, we noted that photoactivation is accompanied by numerous "photon bursts" (Figures 2E and S3, and Supporting Movie) until saturation of the PL intensity occurred (and vice versa). These results imply that a large number of light-emitting defect sites were formed on the surface and deactivated with a characteristic lifetime. However, reliable evidence to fully explain the mechanism was not obtained in the present study, and further investigation will be required for a deeper understanding of the photon bursts during the photoactivation and deactivation processes.

Next, we examined energy transfer from the trapped exciton at the surface to the doped Eu^{3+} ions. Figure 3A shows the time evolution of the PL spectra observed for a single TiO_2:Eu^{3+} nanoparticle (or aggregate) under an Ar atmosphere. Only the PL bands due to Eu^{3+} were observed immediately after laser irradiation, and then the PL band from the trapped exciton appeared in the visible region (500–750 nm) and increased over time. The PL bands attributed to the $^5D_0 \rightarrow {}^7F_1$ and $^5D_0 \rightarrow {}^7F_2$ transitions increased and decreased with increasing irradiation time, respectively (Figure 3B). The time evolution of the R value also seems to be synchronized with the photoactivation event (Figure 3C). This contains information that is difficult or impossible to obtain from ensemble experiments, since each particle or aggregate behaves differently (Figure S4). Such a spectral change was not observed for both 405-nm excitation of TiO_2:Eu^{3+} in air (Figure S5) and 532-nm excitation (i.e., the $^7F_{0,1} \rightarrow {}^5D_1$ transition) of TiO_2:Eu^{3+} in Ar (data not shown).

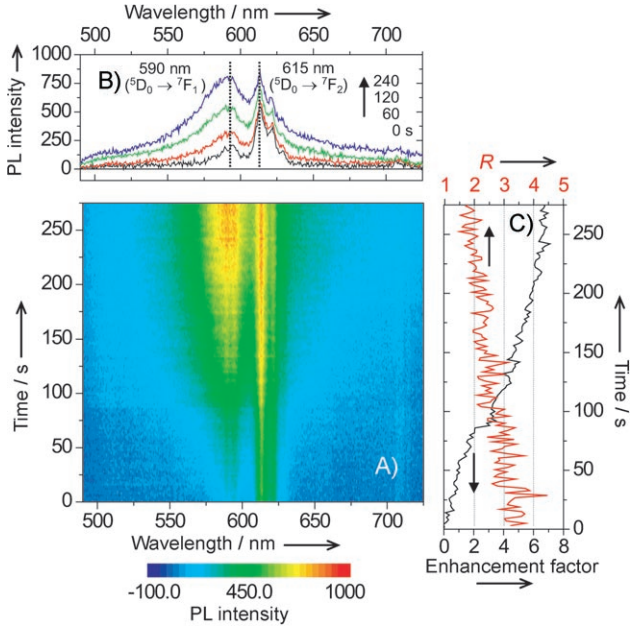

Figure 3. Time evolutions of the PL spectra (A and B) obtained during 405-nm laser excitation for a single TiO_2:Eu^{3+} nanoparticle (or aggregate) under an Ar atmosphere. C) Time traces for the enhancement factor, which is calculated by dividing the differential PL intensity by the original intensity, obtained at 550 nm (black line) and R values (red line).

Based on the above results and discussion, we propose the following PL mechanisms: First, visible color centers, most probably, trapped electrons (e_{tr}^-) in the vacancy defect sites, are generated by intrinsic and/or extrinsic excitation of TiO_2 nanoparticles under 405-nm laser irradiation [reactions (2)–(4)]. Both e_{free}^- and e_{tr}^- can then recombine with the photogenerated holes ($h_{free/tr}^+$) to produce PL in the UV and visible regions, respectively [reaction (5)]. In our experimental setup, only the latter could be detected. The quenching of e_{free}^- by O_2 molecules consequently results in decreased PL from the trapped excitons [reaction (6)]. Free excitons should excite both the interior and surface-located Eu^{3+} ions, while trapped excitons at the surface would only excite the surface-located Eu^{3+} ions [reactions (7) and (8)]. This interpretation is supported by the fact that photoactivation of color centers in the TiO_2 host, that is, formation of trapped excitons at the defect sites, is accompanied by a significant decrease in R (Figure 3).

$$TiO_2 + h\nu(405\ nm) \rightarrow e_{free}^- + h_{free}^+ \text{ (intrinsic absorption)} \quad (2)$$

$$e_{free}^- \rightarrow e_{tr}^- \text{(color centers)} \quad (3)$$

$$e_{tr}^- \text{(color centers)} + h\nu(405\ nm) \rightarrow e_{free}^- \text{ (extrinsic absorption)} \quad (4)$$

$$e_{tr}^- \text{(color centers)} + h_{free/tr}^+ \rightarrow PL \text{ (trapped exciton emission)} \quad (5)$$

$$e_{free}^- + O_2\text{(surface)} \rightarrow O_2^{\cdot -}\text{(surface)} \quad (6)$$

$$Eu^{3+}\text{(interior/surface)} + \text{free exitons} \rightarrow PL(^5D_0 \rightarrow {}^7F_j) \quad (7)$$

$$Eu^{3+}\text{(surface)} + \text{trapped excitons} \rightarrow PL(^5D_0 \rightarrow {}^7F_j) \quad (8)$$

In conclusion, we have clarified the defect-mediated PL dynamics of pure and Eu^{3+}-doped TiO_2 nanoparticles using single-particle PL spectroscopy. The PL spectra and time traces of individual nanoparticles or aggregates revealed that the PL band originating from defects at the TiO_2 surface appears in the visible region with numerous photon bursts on photoirradiation with a 405-nm laser under an Ar atmosphere. Energy transfer from defects to surface-located Eu^{3+} ions is experimentally suggested by the fact that a significant decrease in R is observed during the photoactivation processes. Our findings and methodology should provide further insight into the mechanisms of charge and energy transfer in hybrid inorganic nanomaterials.

Experimental Section

Pure (undoped) and Eu^{3+}-doped TiO_2 nanoparticles were synthesized by the reported procedures.[2d] In a typical method, the liquid precursor (a mixture of titanium tetra-*n*-butoxide (TTBO), diethanolamine, europium(III) nitrate, citric acid, etc.) was delivered by a peristaltic pump into the center of the plasma plume through an atomization probe. The TiO_2 nanoparticles formed by rapid oxidation of the atomized liquid precursor by Ar/O_2 thermal plasma mainly deposit on the filter and the inner walls of the reactor. The flow rate of

the liquid precursor was controlled at 4.5 g min^{-1}, which corresponds to 4.5×10^{-3} mol min^{-1} in terms of TTBO. The atomization probe was water-cooled to resist the extreme temperature of the plasma, and the precursor was atomized into mists at its tip by Ar carrier gas flowing through the probe at 5 L min^{-1}. The Ar/O_2 thermal plasma was generated by mixing O_2 gas with the Ar sheath. The total flow rate of the sheath gas (Ar + O_2) was set at 90 L min^{-1}. Characterization of particles is given in reference [2d]. The atomic force microscopy (AFM, Seiko Instruments, Inc., SPA400-DFM, SI-DF20) and transmission electron microscopy (TEM, JEOL JEM-2100F) images indicated that the mean particle size of the material was about 10 nm (Figure S1).

To explore surface effects on the spectral characteristics, the nanoparticles were embedded in polar (poly(vinyl alcohol), PVA) or nonpolar (polystyrene, PS) matrices. Approximately 0.5 mg of the TiO_2:Eu^{3+} powder was mixed with a toluene solution (300 μL) containing octadecyltrimethoxysilane (10 μL, Aldrich). The mixture was then sonicated for 20 min and allowed to stand for 12 h under an Ar atmosphere. The resulting slurry was centrifuged and washed with fresh toluene to remove any unattached silane molecules. Samples for the single-particle experiments were prepared by spin coating a toluene solution (40 μL) of the modified TiO_2:Eu^{3+} powder and PS (M = 287 000, 5 g L^{-1}) on a clean cover glass at 2000 rpm for 50 s.

For the single-particle PL measurements, the cover glasses (22 × 22 mm) were purchased from Fisher Scientific or Matsunami Glass and cleaned by sonication in a 20% detergent solution (As One, Cleanace) for 6 h, followed by repeated washing with running water for 30 min. Finally, the cover glasses were washed with Milli-Q water. An aqueous suspension of TiO_2:Eu^{3+} nanoparticles (1 mg mL^{-1}, pH 3, HNO_3(aq), 40 μL) was coated onto the clean cover glass by spin coating at 2000 rpm for 50 s. The sample was enclosed in a homemade glove box, and the oxygen concentration inside the box was adjusted by an Ar gas purge.

The experimental setup for single-particle PL measurements is based on an Olympus IX71 inverted fluorescence microscope. Continuous-wave light emitted from a 405-nm diode laser (Olympus, LD405, 0.5 kW cm^{-2}) that passed through an objective lens (Olympus, UPlanSApo, 1.40 NA, 100×) after reflection at a dichroic mirror (Olympus, DM455) was used to excite the nanoparticles. The emission from single nanoparticles or aggregates on the cover glass was collected by an oil-immersion microscope objective, magnified by the built-in 1.6× magnification changer (thus, net magnification was 160×), passed through an emission filter (Olympus, BA475) to remove the undesired scattered light, and intensified by an image intensifier (Hamamatsu Photonics, C8600-03) coupled to a CCD camera (Hamamatsu Photonics, C3077-70). The images were converted into an electronic movie file at a video frame rate of 30 frames per second by using a ADVC 1394 video capture board (Canopus). A number of luminescent spots were analyzed by means of the mean gray scale in the region of interest (typically 3 × 3 pixels) by using custom-made software (Library, Gray Val32) or ImageJ software (http://rsb.info.nih.gov/ij/).

For spectroscopy, only the emission that passed through a slit entered the imaging spectrograph (Acton Research, SP-2356) equipped with an electron-multiplying charge coupled device (EM-CCD) camera (Princeton Instruments, PhotonMAX:512B). The width of the slit was 200 μm, which corresponds to 1.25 μm at the specimen, because the images at the slit were magnified by 160×. The spectra were typically integrated for 2 or 5 s. The spectrum detected by the EM-CCD camera was stored and analyzed on a personal computer. All experimental data were obtained at room temperature.

Received: February 1, 2008
Published online: June 11, 2008

Keywords: fluorescence spectroscopy · lanthanides · nanostructures · photochemistry · single-nanoparticle studies

[1] For example, G. Blasse, B. C. Grabmaier in *Luminescent Materials*, Springer, Berlin, **1994**.

[2] a) A. Conde-Gallardo, M. García-Rocha, I. Hernández-Calderón, R. Palomino-Merino, *Appl. Phys. Lett.* **2001**, *78*, 3436–3438; b) K. L. Frindell, M. H. Bartl, M. R. Robinson, G. C. Bazan, A. Popitsch, G. D. Stucky, *J. Solid State Chem.* **2003**, *172*, 81–88; c) C. W. Jia, E. Q. Xie, J. G. Zhao, Z. W. Sun, A. H. Peng, *J. Appl. Phys.* **2006**, *100*, 023529; d) J.-G. Li, X. Wang, K. Watanabe, T. Ishigaki, *J. Phys. Chem. B* **2006**, *110*, 1121–1127, and references therein.

[3] a) S. A. Empedocles, M. G. Bawendi, *Science* **1997**, *278*, 2114–2117; b) K. T. Shimizu, R. G. Neuhauser, C. A. Leatherdale, S. A. Empedocles, W. K. Woo, M. G. Bawendi, *Phys. Rev. B* **2000**, *63*, 205316; c) R. E. Palacios, F.-R. F. Fan, J. K. Grey, J. Suk, A. J. Bard, P. F. Barbara, *Nat. Mater.* **2007**, *6*, 680–685.

[4] a) M. D. Barnes, A. Mehta, T. Thundat, R. N. Bhargava, V. Chhabra, B. Kulkarni, *J. Phys. Chem. B* **2000**, *104*, 6099–6102; b) R. Rodrigues-Herzog, F. Trotta, H. Bill, J.-M. Segura, B. Hecht, H.-J. Güntherodt, *Phys. Rev. B* **2000**, *62*, 11163–11169; c) A. P. Bartko, L. A. Peyser, R. M. Dickson, A. Mehta, T. Thundat, R. Bhargava, M. D. Barnes, *Chem. Phys. Lett.* **2002**, *358*, 459–465.

[5] a) The volume fraction of total ions on the surface of nanocrystalline TiO_2:Eu^{3+} is calculated by using $\{[4/3\pi r^3-4/3\pi(r-\delta)^3]/4/3\pi r^3\}\times100$, where δ is the assumed surface thickness of 0.4 nm (the length of Ti–O bonds is 0.196 nm)[5b] and r is the particle radius (5 nm). For example, the volume fraction of total ions at the surface is estimated to be about 22%; b) V. Swamy, D. Menzies, B. C. Muddle, A. Kuznetsov, L. S. Dubrovinsky, Q. Dai, V. Dmitriev, *Appl. Phys. Lett.* **2006**, *88*, 243103.

[6] a) K. Riwotzki, M. Haase, *J. Phys. Chem. B* **1998**, *102*, 10129–10135; b) G. Blasse, *Prog. Solid State Chem.* **1988**, *18*, 79–171.

[7] a) J. F. Suyver, R. Meester, J. J. Kelly, A. Meijerink, *Phys. Rev. B* **2001**, *64*, 235408; b) J. F. Suyver, R. Meester, J. J. Kelly, A. Meijerink, *Phys. Rev. B* **2002**, *66*, 079901.

[8] In fact, no significant concentration quenching was observed in the low concentration range of Eu^{3+} ions (< 0.5 atom%) at the bulk level. At the higher dopant concentrations (> 0.5 atom%), however, most of the Eu^{3+} ions are expelled during the cooling processes of the TiO_2 melt droplets because of their very limited solubility in TiO_2, and thus $Eu_2Ti_2O_7$ pyrochlore is formed.[2d]

[9] J. Grausem, M. Dossot, S. Cremel, B. Humbert, F. Viala, P. Mauchien, *J. Phys. Chem. B* **2006**, *110*, 11259–11266.

[10] R. Helmy, A. Y. Fadeev, *Langmuir* **2002**, *18*, 8924–8928.

[11] Anatase and rutile have site symmetries for Ti^{4+} of D_{2d} and D_{2h}, respectively. Thus, the substitution of Eu^{3+} for Ti^{4+} creates oxygen vacancies and lattice distortions in the TiO_2 host which result in the increased asymmetric ratio. The formation of Eu^{3+}-O_2^--Ti^{4+} bonds would increase the degree of covalence between Eu and O, since the Ti^{4+} ion has a larger radius and lower electronegativity. These structural features may partially explain the observed difference in R.

[12] a) Sekiya et al. reported that the visible PL spectrum consists of three components centered at about 517, 577, and 636 nm, which are assigned to excitons bound to partially reduced titanium ions, self-trapped excitons through an exciton–lattice interaction, and oxygen vacancies, respectively.[12b,c] See references [12c–e] for lifetimes of the photogenerated charge carriers and trapped species. It is also noteworthy that no PL band in the near-infrared region due to the intrinsic defects from the rutile TiO_2 was observed under air and Ar atmospheres, although the present undoped TiO_2 and TiO_2:Eu^{3+} powders contain 22 and 31 wt% of rutile, respectively; b) T. Sekiya, S. Kamei, S. Kurita, *J. Lumin.* **2000**, *87–89*, 1140–1142; c) T. Sekiya, M. Tasaki, K. Wakabayashi, S. Kurita, *J. Lumin.* **2004**, *108*, 69–73; d) N. Serpone, D. Lawless, R. Khairutdinov, E. Pelizzetti, *J. Phys.*

Chem. **1995**, *99*, 16655 – 16661; e) T. Tachikawa, M. Fujitsuka, T. Majima, *J. Phys. Chem. C* **2007**, *111*, 5259 – 5275, and references therein.

[13] V. N. Kuznetsov, N. Serpone, *J. Phys. Chem. C* **2007**, *111*, 15277 – 15288.

[14] a) S. R. Cordero, P. J. Carson, R. A. Estabrook, G. F. Strouse, S. K. Buratto, *J. Phys. Chem. B* **2000**, *104*, 12137 – 12142; b) Y. Wang, Z. Tang, M. A. Correa-Duarte, L. M. Liz-Marzán, N. A. Kotov, *J. Am. Chem. Soc.* **2003**, *125*, 2830 – 2831; c) T. Uematsu, S. Maenosono, Y. Yamaguchi, *J. Phys. Chem. B* **2005**, *109*, 8613 – 8618; d) S. F. Lee, M. A. Osborne, *J. Am. Chem. Soc.* **2007**, *129*, 8936 – 8937.

[15] a) The quantum yields for the generation of $O_2^{\bullet-}$ and $^1O_2$, which is most probably generated by the charge-recombination reaction between $O_2^{\bullet-}$ and photogenerated holes, are reported to be about 0.4[15b] and 0.2–0.3,[15c] respectively, for various TiO_2 photocatalysts in air; b) K. Ishibashi, A. Fujishima, T. Watanabe, K. Hashimoto, *J. Phys. Chem. B* **2000**, *104*, 4934 – 4938; c) T. Daimon, Y. Nosaka, *J. Phys. Chem. C* **2007**, *111*, 4420 – 4424.

[16] a) Unfortunately, we cannot perform more quantitative analysis, because there is no report of the absorption cross-section and PL quantum yield of color centers. For the intrinsic absorption of TiO_2, however, the excitation rate (k_{ex}) is roughly estimated to be about $10^5\ s^{-1}$ according to the following equation: $k_{ex} = N_{ph}\cdot\sigma$, where N_{ph} is the number of photons ($1\times10^{21}\ cm^{-2}s^{-1}$) and σ is the absorption cross-section ($5\times10^{-17}\ cm^2$). Here, the σ value is obtained from $\sigma = k_{abs}\cdot V_{particle}$, where k_{abs} is the absorption coefficient ($10^2\ cm^{-1}$, near the band edge of the fundamental absorption of TiO_2)[16b] and $V_{particle}$ is the particle volume ($5\times10^{-19}\ cm^3$, $r = 5$ nm); b) A. V. Emeline, V. K. Ryabchuk, N. Serpone, *J. Phys. Chem. B* **1999**, *103*, 1316 – 1324.

[17] a) The photon energy up-conversion of mid-gap energy levels originating from oxygen vacancies[17b] may be involved in the photoactivation processes; b) N. D. Abazović, M. I. Čomor, M. D. Dramićanin, D. J. Jovanović, S. P. Ahrenkiel, J. M. Nedeljković, *J. Phys. Chem. B* **1999**, *103*, 1316 – 1324.

